Significance of micropores for removal of hydrogen sulfide from oxygen-free gas streams by activated carbon

Bin Liu (liubin_nj@126.com)
Nanjing Forestry University
Songlin Zuo
Nanjing Forestry University

Research Article

Keywords: activated carbon, micropores, hydrogen sulfide, adsorption, oxygen-free

Posted Date: September 16th, 2022

DOI: https://doi.org/10.21203/rs.3.rs-2061433/v1

Abstract

Activated carbon materials are widely used adsorbents for removal of hydrogen sulfide (H_2S) during purification of gas streams. Five commercially available wood-, coal-, and coconut shell-based activated carbons, prepared by phosphoric acid activation and steam activation, were chosen as adsorbents. The removal of H_2S by these materials was studied by plotting breakthrough curves to determine the effect of pore structure on H_2S adsorption from an oxygen-free gas stream. Conventional catalyst-loaded activated carbons were not as effective under these conditions compared with H_2S removal from an oxygen-containing stream. The results showed that adsorption of H_2S by activated carbon under oxygen-free conditions was dependent on the microporous structure, particularly micropores with size of 1 nm. The H_2S breakthrough capacity of CS-3 was 0.026 g/cm^3 under oxygen-free conditions. Compared with conventional KOH- and CuO-loaded activated carbons, the steam activated materials with highly developed micropore structures were better adsorbents for H_2S removal because of their high adsorption capacities and reduced fire risk. Moreover, it was found that pre-adsorption or co-adsorption of carbon tetrachloride led to poisoning of the activated carbon for H_2S adsorption.

1. Introduction

Hydrogen sulfide (H_2S) is an acidic and poisonous gas that is frequently found at various concentrations in industrial gas streams such as natural gas, fermentation gas, syngas and coal-derived gas (Tian et al., 2021; Lin et al., 2021; Andrade et al., 2020; Kandola et al., 2018; Castellini et al., 2020). It is problematic in industrial processes because it poisons catalysts and readily corrodes metallic equipment and pipelines. Accordingly, removal of H_2S from industrial gas streams is an indispensable step in areas such as semiconductor manufacture, high quality oil gas and green catalysis (Zagoruiko et al., 2021). Adsorption is the most commonly used method to remove H_2S from gas streams containing concentrations typically below 100 ppm.

Activated carbon is the most widely used adsorbent for H_2S in the purification of gas streams (Li et al., 2022; Li et al., 2020; Yang et al., 2020; Choudhury et al., 2020). Generally, removal of H_2S requires that the activated carbon is loaded with catalyst, which is commonly an alkaline substance or metal oxide, because the pristine activated carbon has poor adsorption capacity for H_2S (Habeeb et al., 2016; Yu et al., 2019; Anisuzzama et al., 2014; Rattanaphan et al., 2020; Georgiadis et al., 2020). Moreover, extensive investigations have demonstrated that H_2S removal by activated carbon involved complex physical and chemical processes. Therefore, the adsorption capacity of activated carbon for H_2S depends not only on its physicochemical properties but also the adsorption parameters (Choi et al., 2008; Zeng et al., 2020; Zhang et al., 2020). In particular, in the presence of oxygen, H_2S can be oxidized to S, SO_3^{2-} or SO_4^{2-} species during adsorption by activated carbon impregnated with catalyst (Zagoruiko et al., 2018; Qin et al., 2012; Ciahotny et al., 2019), resulting in remarkably enhanced removal of H_2S. Accordingly, air or oxygen is a key factor in the removal of H_2S by activated carbon and thus usually pumped into the gas stream for industrial desulfurization.

However, oxygen and air are not permitted even at quite low concentrations in some gas streams, including natural gas, gaseous carbon dioxide in the beverage industry and supercritical gas. In such oxygen-free conditions, the adsorption capacity of activated carbon for H_2S is dramatically decreased even if catalyst-loaded activated carbon is used. More unfavorably, the H_2S-saturated activated carbon readily ignites during replacement of used adsorbent due to rapid oxidation in air (Xiao et al., 2008; Karthikeyan et al., 2015). Consequently, development of efficient H_2S removal technology using activated carbon in oxygen-free conditions is desirable for industrial desulfurization. Based on the adsorption mechanism of activated carbon, it can be inferred that surface chemistry and pore structure determine the adsorption capacity for H_2S under oxygen-free conditions. It is generally accepted that a basic surface greatly benefits adsorption of acidic H_2S (Shen et al., 2019; Borguet et al., 2005; Bagreev et al., 2004). However, the effect of pore structure has yet to be addressed in detail. This investigation focused on the effect of the micropore structure of activated carbon on the ability to remove H_2S based on detailed structural analysis. The results demonstrated the significance of micropores of different sizes in the adsorption of gaseous H_2S by activated carbon, providing new insight into the adsorption process.

2. Experimental

2.1 Activated carbon adsorbents

Five commercially available activated carbons were selected as adsorbents. These included three coconut shell-based materials with different pore structures (CS-1, CS-2 and CS-3), one bituminous-based activated carbon (BS-1) and one wood-based activated carbon (WS-1), which were all purchased from Purestar, China. CS-1, CS-2, CS-3 and BS-1 are manufactured by steam activation and WS-1 is produced by phosphoric acid activation. All of the materials were crushed and sieved to obtain particles of 1.7–3.35 mm.

The activated carbons were modified by impregnating with a solution of $Cu(NO_3)_2$ or KOH solution. The impregnated Cu^{2+} activated carbons were heat treated under N_2 atmosphere at 450°C for 1 h to give 8% CuO-loaded activated carbons. The KOH-impregnated activated carbons were dried in an oven at 85°C. The resultant impregnated activated carbons were denoted as C-CuO and C-KOH.

2.2 Pore size analysis

Nitrogen adsorption-desorption tests were performed at 77 K using an adsorption analyzer (Autosorb IQ10, Quantachrome, USA). The surface area was calculated using the Brunauer-Emmett-Teller (BET) equation and the total pore volume was obtained at a relative pressure of 0.99. The mesopore volume was obtained using the Barrett, Joyner, and Halenda method. The micropore to mesopore size distribution curves were analyzed using the quenched solid density functional theory (QSDFT) method in terms of the adsorption branch. The ratios of pore volumes of different sizes to the total pore volume were also evaluated based on the pore size distribution of the activated carbons.

2.3 Adsorption test

The breakthrough curves were tested in a vertical adsorption tube (24 · 230 mm). Nitrogen containing 1% v/v H_2S was used as the gas stream for testing breakthrough curves, which was obtained by diluting raw 5% v/v H_2S with nitrogen or carbon tetrachloride (CTC)-loaded nitrogen. The gas stream was calibrated and monitored to maintain a total flow rate of 1450 ± 20 mL/min. All tests used the same carbon volume to keep the same contact time of 5 s. The stream flow was maintained until a breakthrough of 50 ppmv was indicated. The time elapsed from the start to breakthrough was recorded. The H_2S detector was provided by Handa Technology (HD-P900-H_2S). The H_2S breakthrough capacities (BTC) of the adsorbents were calculated by integrating the areas of the breakthrough curves, expressed as the amount (g) of H_2S removed from the vapor stream per volume (cm^3) of carbon. The saturated adsorption capacity (SAC) was calculated by increased weight, expressed as the amount (g) of H_2S removed from the vapor stream per weight (g) of carbon.

$$BTC = \frac{\int_0^t v \cdot (C_0 - C_t)dt}{V} = \frac{vC_0t - \int_0^t vC_tdt}{V}$$

BTC = breakthrough capacity (g/cm^3)

v = flow rate (cm^3/min)

C_0 = initial H_2S concentration (ppmv)

C_t = breakthrough concentration at time t (ppmv)

V = volume of activated carbon (cm^3)

2.4 Ignition temperature testing

The ignition temperatures of the activated carbons were determined according to the method described in the national testing standard of activated carbons GB/T 7702.9–2008. The activated carbon was first placed in a vertical tube in an ignition point analyzer (FMX-K8, ZhongHuiTian Cheng, China) in direct contact with an air steam. The air stream was slowly heated until the activated carbon began to ignite. The temperatures of the carbon bed and the air entering the bed were recorded. The ignition temperature is defined as the point at which the carbon temperature suddenly rises above the temperature of the air entering the bed.

3. Results And Discussion

3.1 Pore structures of activated carbons

Figure 1(a) shows the N_2 adsorption/desorption isotherms of the activated carbons. It can be seen that CS-1, CS-2 and CS-3 all exhibited type I adsorption isotherms with no apparent hysteresis loop, indicative of predominantly micropore structures. The WS-1 and BS-1 activated carbons exhibited type IV adsorption isotherms, which had high adsorption capacity before the knee point in the curves and exhibit an obvious hysteresis loop. The results demonstrated that WS-1 and BS-1 had microporous/mesoporous structures. The pore parameters are listed in Table 1. The data further confirmed that CS-1, CS-2 and CS-3 had highly

developed microporous structures while WS-1 and BS-1 had almost negligible numbers of mesopores. WS-1 was prepared by phosphoric acid activation, a chemical activation method, and therefore contained a high proportion of mesopores. The pore size distributions of these activated carbons are presented in Fig. 1(b). A comparison of the pore size distribution curves indicated that the pores in CS-1, CS-2 and CS-3 were predominantly less than 3 nm, while WS-1 and BS-1 had a wide size distribution including larger than 5 nm but with a considerable number of pores with sizes less than 2 nm. A further observation shown in the figure insert demonstrated that pores of less than 2 nm diameter were predominant in CS-1, CS-2 and CS-3, which shows that WS-1 had the largest pore volume.

Table 1
The porous parameters of the activated carbons

	BET surface area (m^2/g)	Total pore volume (cm^3/g)	Micropore volume (cm^3/g)	Mesopore volume (cm^3/g)	Average pore size nm
WS-1	1315	1.149	0.359	0.665	3.49
BS-1	1100	0.818	0.369	0.381	2.97
CS-1	1156	0.626	0.404	0.152	2.09
CS-2	1371	0.645	0.590	0.032	1.87
CS-3	1792	0.835	0.728	0.078	1.86

3.2 Effect of pore size on H_2S adsorption

Figures 2 and 3 show the H_2S breakthrough curves and saturated adsorption capacities of the activated carbons. From the breakthrough curves, the H_2S BTC values of WS-1, BS-1, CS-1, CS-2 and CS-3 were 0.006, 0.01, 0.018, 0.021 and 0.026 g/cm^3, respectively. Clearly, the breakthrough of H_2S gas stream through an activated carbon column varied greatly dependent on the activated carbon species. The CS-3 activated carbon column exhibited the longest breakthrough time of about 118 min, while WS-1 was shortest at about 27 min. It can be seen that the adsorption capacity of CS-3 toward H_2S was about 4.4 times that of WS-1 in the fixed-bed adsorption process. This indicated that it had about 4.4 times the adsorption capacity in an adsorption column. The great difference in the adsorption capacities of WS-1 and CS-3 could be attributed to differences in their surface chemistry and pore structures. The WS-1 activated carbon, prepared by phosphoric acid activation of wood sawdust, had an acidic surface that was not conducive to the adsorption of acidic H_2S. In contrast, CS-3, obtained by steam activation of coconut shell charcoal, had a basic surface that favored adsorption of H_2S. Moreover, we found that micropores played a key role in the adsorption of H_2S. CS-3 had a much higher micropore volume (0.728 cm^3/g) than that of WS-1 (0.359 cm^3/g). Comparing CS-1, CS-2 and CS-3 activated carbons, which were all prepared by steam activation of coconut shell-based chars, it was found that activated carbon with a higher micropore volume exhibited a longer breakthrough

time. Figure 4 shows that the adsorption capacity of activated carbons in a fixed bed increased almost linearly as the micropore volume increased.

However, it is noteworthy that although there was only a small difference in the micropore volumes of BS-1 and CS-1 (0.369 and 0.404 cm^3/g, respectively), CS-1 exhibited a much longer breakthrough time of 80 min compared to the 45 min of BS-1. The calculated adsorption capacity of CS-1 was also much higher than that of BS-1. This comparison indicated that the micropore size exerted a significant effect on the adsorption of H_2S by activated carbon. In order to further elucidate the effect of micropore size distribution on H_2S adsorption, a regression analysis was conducted. Based on the pore size distribution determined using the QSDFT model, the total pore volumes of the five activated carbons were calculated, together with the volumes of pores with diameters below 1, 2 and 5 nm. All of the results are listed in Table 2. From Table 2, the micropore volume ratios of WS-1 and BS-1 were 31% and 36.5%, respectively, indicating that micropore is not a key feature of WS-1 and BS-1. In contrast, the micropore ratios of CS-1, CS-2 and CS-3 were all greater than 65%, indicating that micropore volume was the major feature of the three activated carbons. The H_2S breakthrough time and saturated adsorption capacity increased as the volume of pores with diameter less than 1 nm increased.

Table 2
Analysis for different range of micropore

Pore range (nm)	WS-1		BS-1		CS-1		CS-2		CS-3	
	Volume (cm^3/g)	Ratio (%)	Volume (cm^3/g)	Ratio (%)	Volume (cm^3/g)	Ratio (%)	Volume (cm^3/g)	Ratio (%)	Volume (cm^3/g)	Ratio (%)
< 1	0.207	16.8	0.241	34.1	0.274	47.9	0.310	52.9	0.332	43.7
< 2	0.382	31	0.258	36.5	0.378	66.1	0.382	65.2	0.495	65.1
< 5	0.596	48.3	0.416	57.8	0.424	74.1	0.449	76.6	0.722	95.0
Total	1.234		0.707		0.572		0.586		0.76	

To analyze the relationship between pore volume and H_2S adsorption capacity, the data were plotted as shown in Fig. 5. From the results, the SAC was significantly increased as the volume of pores with diameter less than 1 nm increased, with the best regression coefficient of 0.9527. The R^2 values were lower for volumes of pores of size less than 2 and 5 nm, indicating that the volume of pores smaller than 1 nm was most strongly correlated with H_2S adsorption capacity. In addition, the slope of the curve for volume of pores smaller than 1 nm versus SAC was greater than those of the other two, which indicated that a small increase of volume of pores smaller than 1 nm could contribute a larger increase of H_2S adsorption capacity.

According to adsorption theory, the suitable adsorption range of an adsorbent for a specific adsorbate is approximately three times the molecular size of the adsorbate (Zhang et al., 2006; Llewellyn et al., 1994; Papadopoulos et al., 2007). The molecular diameter of H_2S is about 0.36 nm (Shah et al., 2017), so the most effective pore size calculated based on adsorption theory is approximately 1 nm. Accordingly, it can be

concluded that the volume of pores with diameter below 1 nm had the most important effect on H_2S adsorption. The larger the volume of pores with diameter less than 1 nm, the greater the H_2S adsorption capacity.

3.3 Importance of micropores on H_2S adsorption

In order to further highlight the importance of micropores in H_2S adsorption, we compared the performance of CS-3 and CS-3 modified by loading with KOH or CuO, which are commonly used to improve the uptake of H_2S by activated carbon. The N_2 adsorption isotherms of CS-3, C-KOH and C-CuO are shown in Fig. 6 and their pore parameters are listed in Table 3. It is evident that the micropore volume of the activated carbon was remarkably reduced by almost 50% after loading with KOH or CuO, especially for pore diameter less than 1 nm. The remarkably reduced number of micropores led to a significant reduction of H_2S adsorption capacity despite the benefit of KOH and CuO loading for chemical adsorption of H_2S by activated carbon, as shown in Fig. 7. This provided further evidence for the importance of micropores in H_2S adsorption. Nevertheless, it should be noted that the adsorption here was under oxygen-free conditions, hampering the ability of KOH and CuO to convert H_2S into S, SO_3^{2-} or SO_4^{2-}, which is the main mechanism for removal of H_2S by these catalysts in a stream containing oxygen or air (Bandosz, 2002; Sitthikhankaew et al., 2014; Xiao et al., 2008).

Table 3
Porous properties of CS-3, C-KOH and C-CuO

	BET surface area (m^2/g)	Total pore volume (cm^3/g)	Micropore volume (cm^3/g)	Pore volume below 1 nm (cm^3/g)
CS-3	1792	0.835	0.728	0.332
C-KOH	1216	0.809	0.389	0.0748
C-CuO	972	0.607	0.361	0.0591

Considering that the gas stream usually contains organic substances other than H_2S, we tested the effect of carbon tetrachloride on the adsorption of H_2S by activated carbon and the results are shown in Fig. 8. Surprisingly, the breakthrough time was sharply decreased to almost zero when CS-1 was pre-saturated with gaseous carbon tetrachloride or the adsorption was conducted with a gaseous mixture of carbon tetrachloride and H_2S. We described this phenomenon as the poisoning of activated carbon for adsorption of H_2S. This was attributed to the adsorbed carbon tetrachloride blocking entry of H_2S molecules into micropores of less than 1 nm diameter, since the molecular size of carbon tetrachloride was 0.59 nm (Sing et al., 2004). and much larger than the 0.36 nm of H_2S. This poisoning phenomenon further illustrated the importance of smaller micropores in the H_2S adsorption process. Understandably, the influence of contaminant gaseous components depended on their molecular dimensions and physicochemical properties, which requires further research. Certainly, much consideration needs to be given to the effects of other components on H_2S removal by activated carbon.

3.4 Risk of spent carbon fire

Based on the above results, it was concluded that activated carbon with highly developed micropores in the size range of less than 1 nm was more favorable than traditional KOH- or CuO-loaded activated carbon for H_2S removal under oxygen-free conditions. In the industrial process, fire risk is another important factor in the use activated carbon for H_2S removal. We therefore examined the ignition temperatures of BS-1and CS-3 microporous activated carbons and the KOH- and CuO-loaded activated carbons, C-KOH and C-CuO, as shown in Table 4. It was found that loading with KOH or CuO led to an obvious decrease in the ignition temperature. This may be due to catalytic oxidation of carbon by air or oxygen in the presence of KOH or CuO. Consequently, when the used adsorbents, that is the H_2S-saturated activated carbons, made direct contact with air, the used C-KOH and C-CuO materials ignited while the used BS-1 and CS-3 did not burn. Clearly, the BS-1 and CS-3 microporous activated carbon materials were safer and exhibit an outstanding advantage in the large-scale industrial process.

Table 4
The safety parameters of CS-3, BS-1, C-KOH and C-CuO.

Samples	Ignition Temperature (°C)	Spent carbon fire
CS-3	407	No
BS-1	459	No
C-KOH	232	Burn Directly
C-CuO	360	Burn Directly

4. Conclusions

The breakthrough curves of the five activated carbon materials, including wood-based activated carbon prepared by phosphoric acid activation, and coal- and coconut shell-based activated carbon prepared by steam activation, showed that micropores with diameters of less than 1 nm were the main contributors to adsorption of H_2S. Compared with conventional KOH- and CuO-loaded activated carbon, the steam activated carbon materials with highly developed micropore structures were more favorable adsorbents for H_2S removal because of advantages such as higher adsorption capacity, longer breakthrough time and reduced fire risk. Furthermore, it was found that pre-adsorption or co-adsorption of carbon tetrachloride led to poisoning of H_2S adsorption by activated carbon, indicating that contaminants in the gas stream could seriously diminish H_2S adsorption by activated carbon.

Declarations

Acknowledgement

This study was funded by the National Key Research and Development Program of China (No.2019YFB1503804).

References

1. Andrade, I.M., Moreno, G., Quijano, G., 2020. Theoretical framework for the estimation of H_2S concentration in biogas produced from complex sulfur-rich substrates. Environmental Science and Pollution Research, 27, 15959–15966.
2. Anisuzzama, S.M., Krishnaiah, D., Joseph, C.G., Abang, S., 2014. Dynamic simulation of hydrogen sulfide adsorption in a packed bed column of activated carbon. Journal of Applied Sciences, 14, 3294–3299.
3. Bagreev, A., Menendez, J.A., Dukhno, I., Tarasenko, Y., Bandosz, T.J., 2004. Bituminous coal-based activated carbons modified with nitrogen as adsorbents of hydrogen sulfide. Carbon, 42, 469–476.
4. Bandosz, T.J., 2002. On the adsorption/oxidation of hydrogen sulfide on activated carbons at ambient temperatures. Journal of Colloid & Interface ence, 246, 1–20.
5. Borguet, E., Kwon, S., Feng, W., Vidic, R., 2005. Adsorption of hydrogen sulfide onto activated carbon fibers: Effect of pore structure and surface chemistry. Environmental Science & Technology, 39, 9744–9749.
6. Castellini, E., Bernini, F., Sebastianelli, L., Sainz-Diaz, C.I., Borsari, M., 2020. Interlayer-confined Cu(II) complex as an efficient and long-lasting catalyst for oxidation of H_2S on Montmorillonite. Minerals. Minerals, 10, 1–13.
7. Choi, D.Y., Lee, J.W., Jang, S.C., 2008. Adsorption dynamics of hydrogen sulfide in impregnated activated carbon bed. Adsorption, 14, 533–538.
8. Choudhury, A., Lansing, S., 2020. Biochar addition with Fe-impregnation to reduce H_2S production from anaerobic digestion. Bioresource Technology, 306, 123121.
9. Ciahotny, K., Kyselova, V., 2019. Hydrogen sulfide removal from biogas using carbon impregnated with oxidants. Energy & Fuels, 33, 5316–5321.
10. Georgiadis, A.G., Charisiou, N.D., Goula, M.A., 2020. Removal of hydrogen sulfide from various industrial gases: A review of the most promising adsorbing materials. Catalysts, 10, 2–36.
11. Habeeb, O.A., Ramesh, K., Ali, G.A.M., 2016. Modeling and optimization for H_2S adsorption from wastewater using coconut shell based activated carbon. Australian Journal of Basic & Applied Sciences, 10, 136–147.
12. Kandola, I., Pogrebnoi, A., Pogrebnaya, T., 2018. Oldoinyo Lengai Volcanic ash for removal of hydrogen sulfide and ammonia from biogas. Journal of Materials Science & Chemical Engineering, 6, 78–93.
13. Karthikeyan, S., Magthalin, C.J., Mahesh, M., Anandan, C., Sekaran, G., 2015. Synthesis of reactive iron impregnated nanoporous activated carbon and its application in anaerobic biological treatment to enhance biodegradability of ortho-phenylenediamine. Journal of Chemical Technology & Biotechnology, 90, 1013–1026.
14. Li, K., Wang, C., Ning, P., Li, K., Sun, X., Song, X., Mei, Y., 2020. Surface characterization of metal oxides-supported activated carbon fiber catalysts for simultaneous catalytic hydrolysis of carbonyl sulfide and carbon disulfide. Journal of Environmental Sciences, 11, 44–54.
15. Li, X., Wang, X.Q., Wang, L.L., Ning, P., Ma, Y.X., Zhong, L., Wu, Y., Yuan, L., 2022. Efficient removal of carbonyl sulfur and hydrogen sulfide from blast furnace gas by one-step catalytic process with modified

activated carbon. Applied Surface Science, 579, 152189.

16. Lin, Y., Li, Y., Xu, Z., Guo, J., Zhu, T., 2021. Carbon consumption and adsorption-regeneration of H_2S on activated carbon for coke oven flue gas purification. Environmental Science and Pollution Research, 28, 60557–60568.
17. Llewellyn, P.L., Grillet, Y., Schuth, F., Reichert, H., Unger, K.K., 1994. Effect of pore size on adsorbate condensation and hysteresis within a potential model adsorbent: M41S. Microporous Materials, 3, 345–349.
18. Papadopoulos, G.K., Petropoulos, J.H., 2007. Model study of the effect of pore structure and condensation on multilayer adsorbate transport in porous media. Langmuir the Acs Journal of Surfaces & Colloids, 23, 12932–12936.
19. Qin, H., Wu, D.X., Wang, Q., 2012. Research on adsorption of H_2S by modified activated carbon. Advanced Materials Research, 463–464, 128–132.
20. Rattanaphan, S., Rungrotmongkol, T., Kongsune, P., 2020. Biogas improving by adsorption of CO_2 on modified waste tea activated carbon. Renewable Energy, 145, 622–631.
21. Shah, M.S., Tsapatsis, M., Siepmann, J.I., 2017. Hydrogen sulfide capture: From absorption in polar liquids to oxide, zeolite and metal-organic framework adsorbents and membranes. Chemical Reviews, 117, 9755–9803.
22. Shen, F., Liu, J., Gu, C., Wu, D., 2019. Roles of oxygen functional groups in hydrogen sulfide adsorption on activated carbon surface: A density functional study. Industrial & Engineering Chemistry Research, 58, 5526–5532.
23. Sing, K.W., Williams, R., 2004. The use of molecular probes for the characterization of nanoporous adsorbents. Particle & Particle Systems Characterization, 21, 71–79.
24. Sitthikhankaew, R., Chadwick, D., Assabumrungrat, S., Laosiripojana, N., 2014. Effects of humidity, O_2, and CO_2 on H_2S adsorption onto upgraded and KOH impregnated activated carbons. Fuel Processing Technology, 124, 249–257.
25. Tian, X.F., Wang, L.M., Zhang, P., Fu, D., Wang, Z.Y., 2021. A high efficient absorbent for the separation of H_2S from low partial pressure coke oven gas. Environmental Science and Pollution Research, 28, 5822–5832.
26. Xiao, Y., Wang, S., Wu, D., Quan, Y., 2008. Catalytic oxidation of hydrogen sulfide over unmodified and impregnated activated carbon, Separation & Purification Technology, 59, 326–332.
27. Xiao, Y., Wang, S., Wu, D., Quan, Y., 2008. Experimental and simulation study of hydrogen sulfide adsorption on impregnated activated carbon under anaerobic conditions. Journal of Hazardous Materials, 153, 1193–1200.
28. Yang, C., Ye, H., Byun, J., Hou, Y., Wang, X., 2020. N-Rich carbon catalysts with economic feasibility for the selective oxidation of hydrogen sulfide to sulfur. Environmental Science and Technology, 54, 12621–12630.
29. Yu, Q.F., Li, M., Ning, P., Yi, H., Tang, X., 2019. Characterization of metal oxide-modified walnut-shell activated carbon and its application for phosphine adsorption: Equilibrium, regeneration, and mechanism studies. Journal of Wuhan University of Technology Mater Sci Ed, 34, 487–495.

30. Zagoruiko, A., Mikenin, P., 2021. Decomposition of hydrogen sulfide into elements in the cyclic chemisorption-catalytic regime. Catalysis Today, 378, 176–188.
31. Zagoruiko, A.N., Vasiliy, S., Gennady, K., 2018. Kinetics of H_2S selective oxidation by oxygen at the carbon nanofibrous catalyst. Reaction Kinetics Mechanisms & Catalysis, 123, 1–15.
32. Zeng, F., Liao, X., Lu, J., Pan, D., Zhang, W., 2020. Effect of iron salt modification on the adsorption of hydrogen sulfide by sludge-based activated carbon. Desalination and Water Treatment, 202, 61–70.
33. Zhang, X., Li, A., Jiang, Z., Zhang, Q., 2006. Adsorption of dyes and phenol from water on resin adsorbents: Effect of adsorbate size and pore size distribution. Journal of Hazardous Materials, 137, 1115–1122.
34. Zhang, Y., Zhang, Z., Liu, X., Liu, L., Peng, J., 2020. Desulfurization process and kinetics of Fe/activated carbon removal of H_2S at low temperature. ChemistrySelect, 5, 8386–8393.

Figures

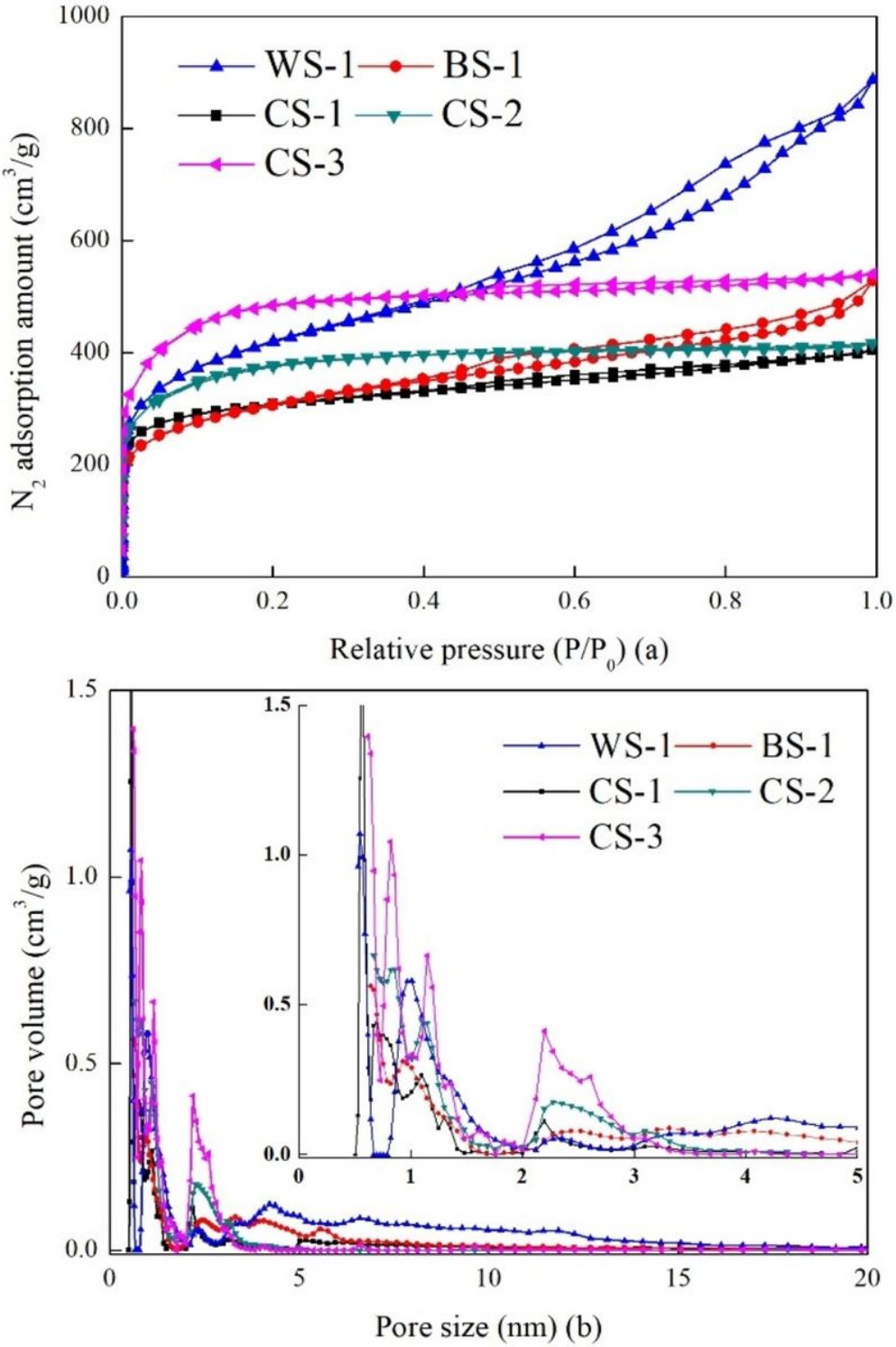

Figure 1

The N_2 adsorption isotherms and pore size distribution of activated carbons

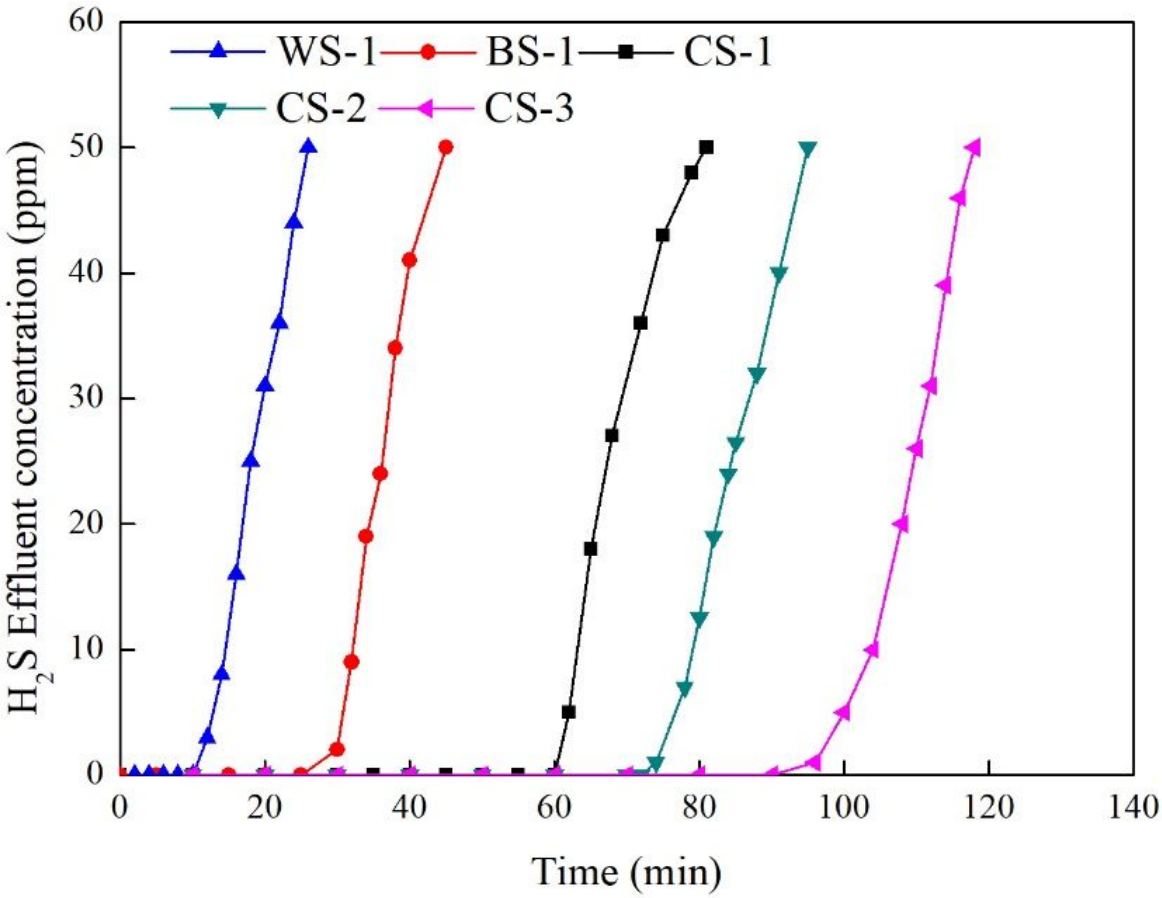

Figure 2

The H_2S breakthrough curves of WS-1, BS-1, CS-1, CS-2 and CS-3

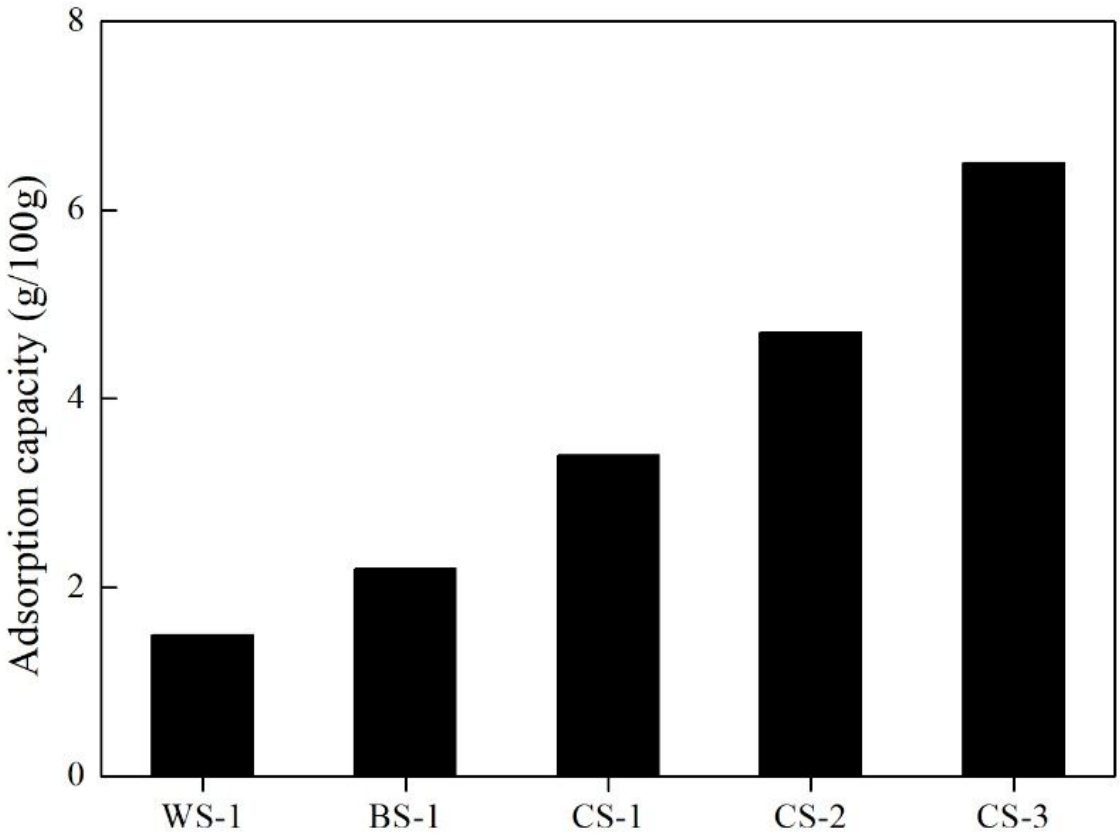

Figure 3

The SAC of WS-1, BS-1, CS-1, CS-2 and CS-3

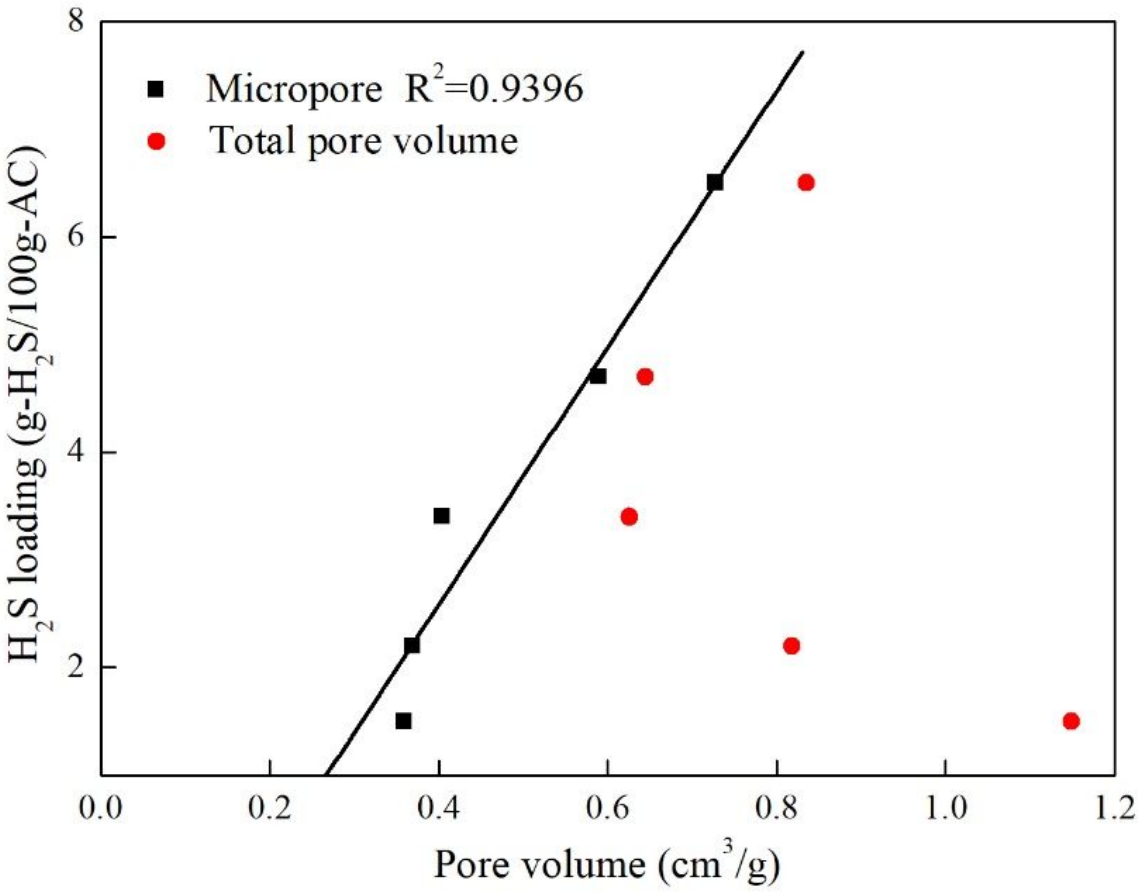

Figure 4

Relation between carbon porous properties and H_2S adsorption capacity.

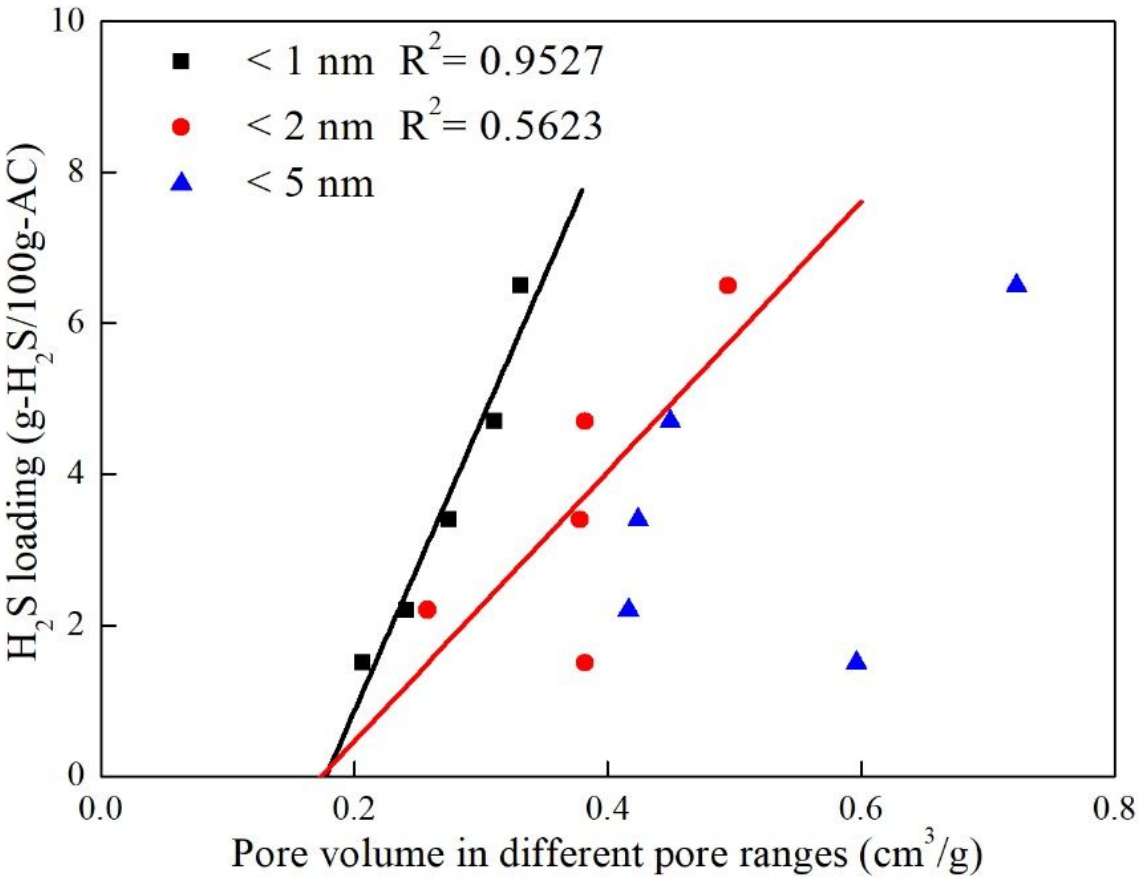

Figure 5

Relation between pore volume and H_2S adsorption capacity.

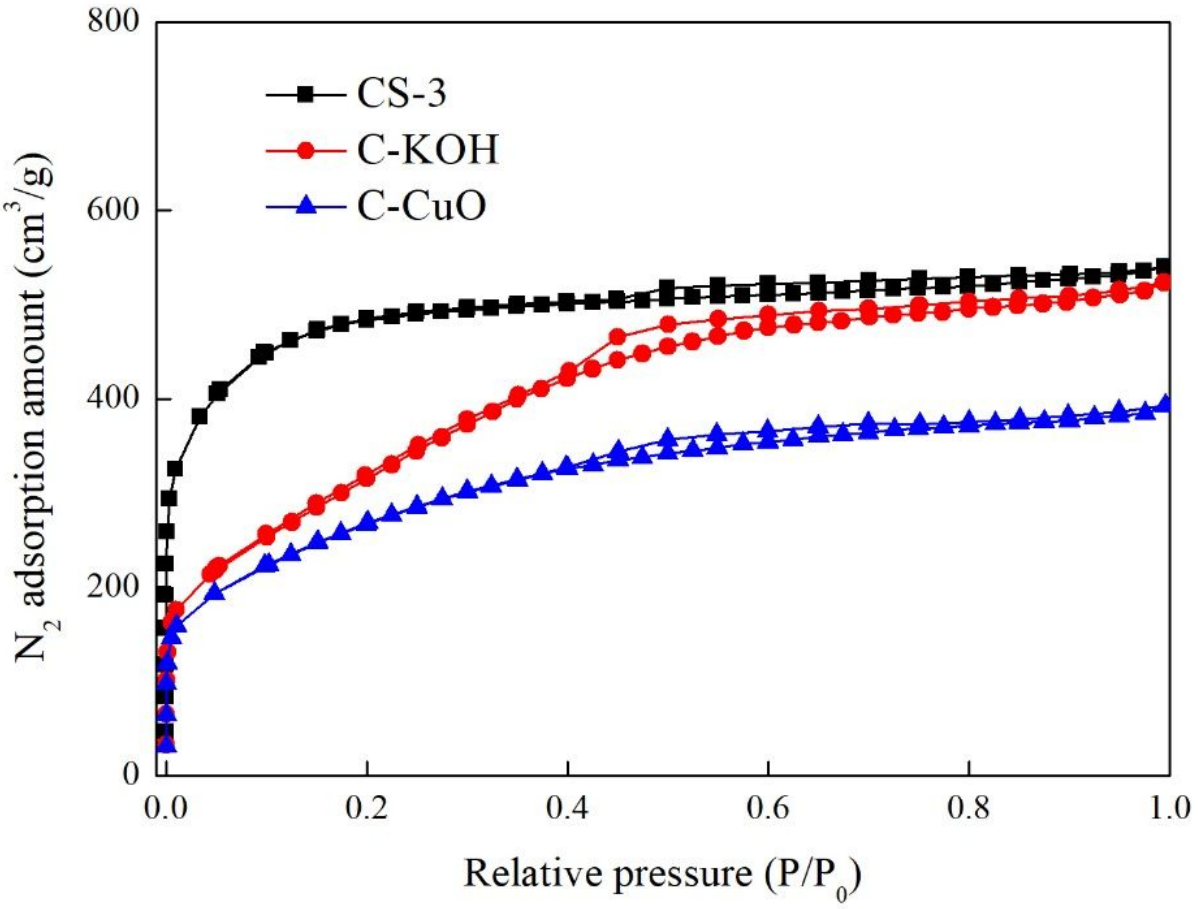

Figure 6

N_2 adsorption isotherms for CS-3, C-KOH and C-CuO

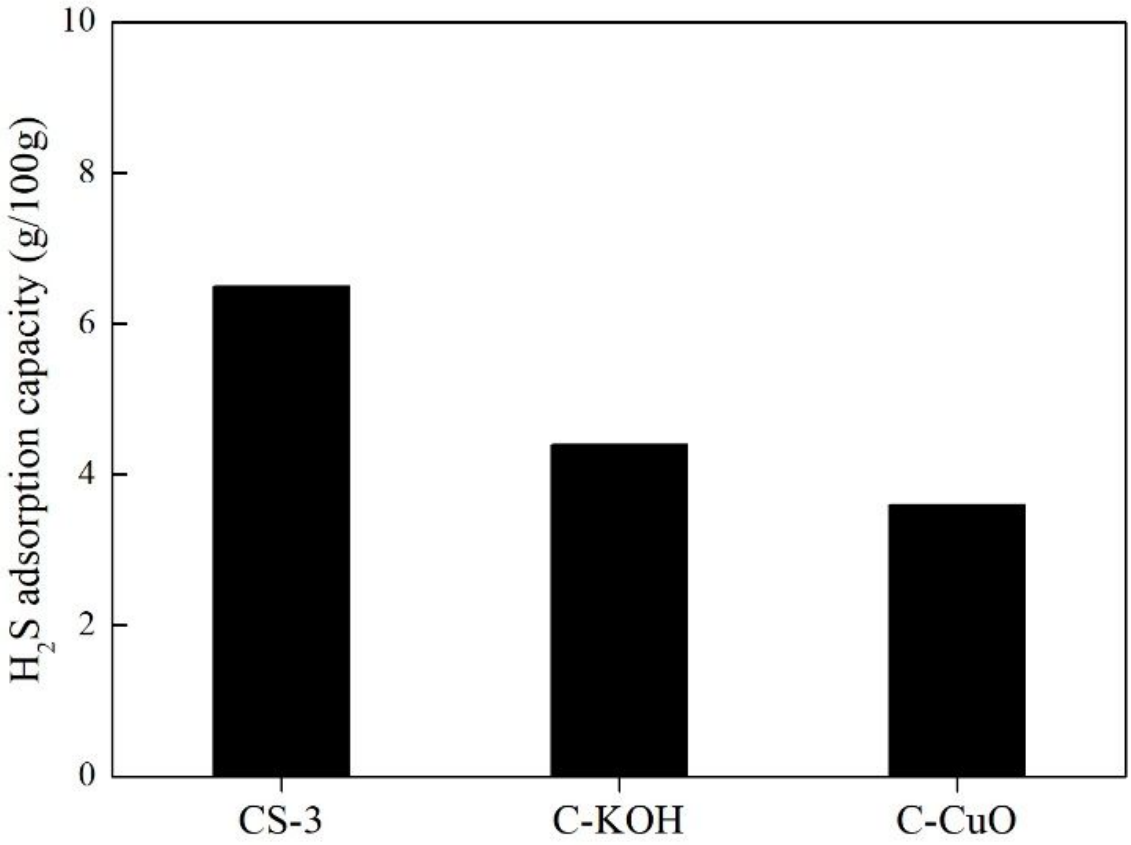

Figure 7

The adsorption capacity of CS-3, C-KOH and C-CuO

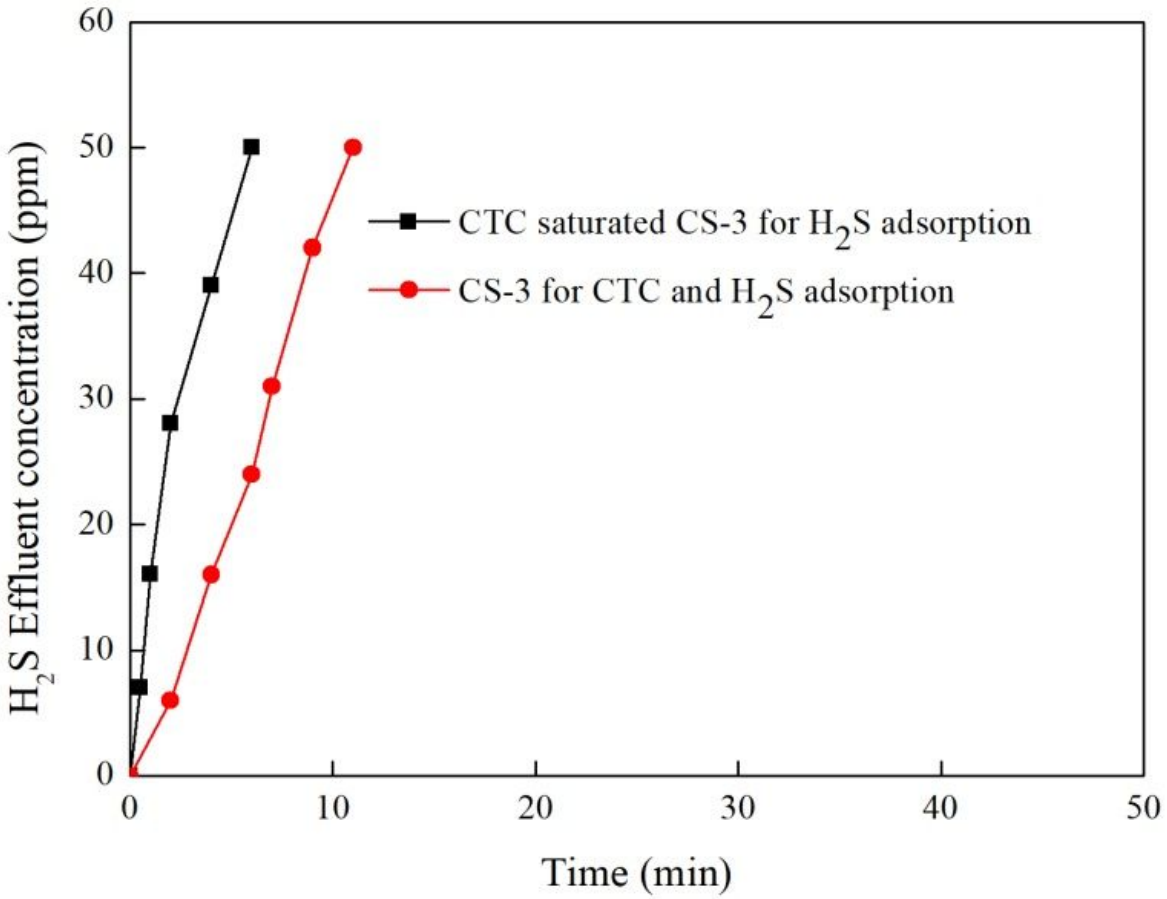

Figure 8

The effect of organic on H_2S adsorption.